THE EVOLUTION OF PRE–MAIN-SEQUENCE STARS

FRANCESCO PALLA
Osservatorio Astrofisico di Arcetri
Largo E. Fermi, 5 - 50125 Firenze, Italy

1. The classical theory of pre–main-sequence evolution

The location of optically visible Pre–Main-Sequence (PMS) stars in the H-R diagram combined with the use of theoretical evolutionary tracks have played a central role in stellar evolution studies since the initial work of Hayashi, Cameron and Iben in the early '60s. Hayashi and his contemporaries lacked a theory of the protostar phase, and therefore could not specify with any degree of confidence the initial conditions for PMS contraction. A simple argument indicated that if the interstellar cloud radiated away little energy during its collapse, the starting values of the stellar radius would be some two orders of magnitude greater than the corresponding main-sequence values (Hayashi 1966). The contraction time, given by the Kelvin-Helmoltz time $\mathrm{t_{KH}} = GM_*^2/R_*L_{\rm surf}$, is so short for these large radii and high surface luminosities that the poorly understood early collapse would be much too brief to affect the subsequent evolution. Adopting the large initial radii, Iben (1965) and Ezer & Cameron (1965) followed numerically the hydrostatic contraction of stars with masses from less than 1 $\mathrm{M_\odot}$ to over 100 $\mathrm{M_\odot}$. The evolution of all stars was thought to be qualitatively the same, with quantitative differences scaling in a simple manner with the stellar mass $\mathrm{M_*}$.

1.1. BASIC RESULTS

Let us first follow the arguments used by Hayashi and others to derive the initial stellar radii. A protostar of mass M_* and radius R_* forms out of cold, nearly static cloud material whose dimensions are enormous compared to R_*. Thus, we may effectively set the initial energy, both mechanical and thermal, to zero. The star itself, however, is a gravitationally bound entity with a *negative* total energy. Some of the energy difference is radiated into space during collapse, while most of the rest goes into dissociating and ionizing hydrogen and helium. We denote this latter, internal component as $\Delta E_{\rm int}$, where

$$\Delta E_{\rm int} \equiv \frac{X\,M_*}{m_H}\left[\frac{\Delta E_{\rm diss}(H)}{2} + \Delta E_{\rm ion}(H)\right] + \frac{Y\,M_*\,\Delta E_{\rm ion}(He)}{4\,m_H}\ . \qquad (1)$$

Here, $\Delta E_{\rm diss}(H) = 4.48$ eV is the binding energy of H_2, $\Delta E_{\rm ion}(H) = 13.6$ eV is the ionization potential of HI, and $\Delta E_{\rm ion}(He) = 75.0$ eV is the energy required to fully ionize helium. The hydrogen and helium mass fractions are taken to be X=0.70 and Y=0.28, respectively. Since the protostar's thermal energy is equal to half the gravitational potential energy by the virial theorem, we may write

$$0 = -\frac{1}{2}\,\frac{G\,M_*^2}{R_*} + \Delta E_{\rm int} + L_{\rm rad}\,t\ , \qquad (2)$$

where $L_{\rm rad}$ is the average luminosity escaping over the formation time t. Suppose that we first take the extreme step of ignoring $L_{\rm rad}$ entirely. Then equation (2) yields the *maximum* radius $R_{\rm max}$ which the protostar could have at any mass M_*. We readily find

$$R_{\rm max} = \frac{G\,M_*^2}{2\,\Delta E_{\rm int}} = 61\ R_\odot\left(\frac{M_*}{M_\odot}\right)\ . \qquad (3)$$

This numerical estimate would change slightly with a more careful treatment of the gravitational energy. No direct observations are available of the true radii of solar-type protostars, but even the youngest and largest T Tauri stars, the immediate descendants of these objects, have radii smaller by an order of magnitude than that predicted by equation (3).

Having established the initial conditions, the classical theory of PMS evolution then predicts that any star contracts due to heat loss at a rate given by

$$L_{\rm surf} = 4\pi R_*^2\sigma T_{\rm eff}^4\ , \qquad (4)$$

where $L_{\rm surf}$ is the surface luminosity and $T_{\rm eff}$ the effective temperature of the star. The star is also fully convective because of the large radius. For a one solar mass star with an effective temperature of about 4000 K, $L_{\rm surf}$ ~600 $L_\odot$ which is much higher than the luminosity that can be carried out radiatively

$$L_{\rm rad} = L_0\left(\frac{M_*}{M_\odot}\right)^{11/2}\left(\frac{R_*}{R_\odot}\right)^{-1/2}\ , \qquad (5)$$

where the precise value of L_0, a luminosity of order 1 $L_\odot$, depends on the star's detailed structure and where it has been assumed that the interior opacity obeys Kramer's Law (Cox & Giuli 1968). Thus, convection spreads inward from the surface (Von Sengbusch 1968).

The path followed by any star in the H-R diagram is the same. Stars contract *homologously* descending along nearly vertical tracks, commonly called *Hayashi tracks*), in a Kelvin-Helmoltz time scale which is much longer than the sound crossing time. Therefore, the star can effectively be considered to be in hydrostatic equilibrium at each instant, despite its slow, or *quasi-static*, contraction. At a certain point, a radiative core develops and the star moves away from the Hayashi track along a radiative track (discovered by Henyey, LeLevier & Levee in 1955), at almost constant luminosity. Eventually, hydrogen ignites in the center and contraction is halted: the PMS star has reached the *Zero-Age-Main-Sequence* (ZAMS). These results were obtained in the pioneering numerical models of Iben (1965) and Ezer & Cameron (1965) which established the *standard* set of PMS tracks in the H-R diagram and which can be found in any textbook on stellar evolution.

Before concluding this introductory section, let remind two fundamental properties discovered in the original derivation by Hayashi. First, stars of a given mass and radius have a minimum surface temperature, the *Hayashi temperature*; second, the Hayashi temperature is insensitive to the stellar radius, so that the convective portions of the tracks are nearly vertical. Both properties reflect the behavior of the opacity of the gas in the outer layers of the star. The minimum surface temperature is due to the steep decline of opacity with falling temperature below the hydrogen ionization zone near 10^4 K. For too low a surface temperature, the outer layers become optically thin, violating the condition that the photosphere be located at an optical depth of order unity from the surface. The extreme temperature sensitivity of the opacity is also responsible for the vertical nature of the Hayashi tracks. At temperatures below 10^4 K, the opacity varies as T^α with α between 7 and 13. Therefore, only a minor change of $T_{\rm eff}$ is needed for a substantial change in the photospheric pressure and entropy (which determine the boundary conditions). For solar-type stars, the effective temperature is about 4000 K. An excellent explanation of the role of the photosphere and entropy structure in determining the basic properties of PMS stars, together with the history of the early developments of PMS theory can be found in the review by Stahler (1988b).

1.2. THE INFLUENCE OF PROTOSTELLAR EVOLUTION

The development of protostar theory has altered the conception of PMS evolution, in particular for stars more massive than solar. Many such stars undergo a transient period of thermal relaxation prior to settling down to the type of evolution envisioned earlier. Furthermore, the union of protostar and PMS theory implies that stars of 100 $M_\odot$ or even 20 $M_\odot$ should have no PMS phase at all. To follow these changes in detail one must know how stars of various masses are built up from collapsing clouds. An exhaustive account of this phase can be found in the reviews by Stahler & Walter (1993) and Palla (1994). Here, it suffices to point out some of the main results, relevant for PMS evolution.

The formation of a protostar from the quiescient conditions typical of dense molecular clouds occurs through the gradual accumulation of the interstellar gas onto an accreting core. This process requires a large decrease in gravitational potential energy. Unlike the basic assumption that leads to the expression for the maximum radius of the protostars (see eq. 3), most of the energy during collapse is radiated away and only a small fraction goes into the thermal energy of the protostar. As suggested early on by Gaustad (1963) and others, the high efficiency of radiative losses keeps the interstellar gas almost isothermal during the dynamical collapse phase. A large fraction of the gravitational energy is radiated in radial or disk accretion shocks that form as a result of the abrupt change in the velocity of the freely-falling gas. If no net energy is absorbed by the circumstellar material, the resulting protostellar luminosity is given to a good approximation by

$$L_{\rm proto} = \frac{G\, M_*\, \dot{M}_{\rm acc}}{R_*}\ , \tag{6}$$

where M_* and R_* are the instantaneous mass and radius of the protostellar core and $\dot{M}_{\rm acc} \equiv dM_*/dt$ is the mass accretion rate. Thus, estimates of the luminosity emitted during this phase rely on the knowledge of two fundamental quantities: the accretion rate and the *mass-radius relation*. The former is determined by the dynamics of the gravitational collapse, while the relation between mass and radius are established by processes occuring in the protostellar interior. The radiation produced at the shock is absorbed, reradiated and thermalized in the optically thick, dusty infalling envelope. Most of the observable radiation is emitted at mid- and far-infrared wavelengths. The exact shape of the emergent spectrum depends on the density and temperature distribution of the dust component, which are set by the dynamics of collapse.

As shown by the first numerical models (e.g. Larson 1969), gravitational collapse occurs in a highly *non-homologous* way. The central regions of the cloud collapse faster than the outer parts, pressure gradients develop fast, and the nonhomology sets in already during the initial isothermal phase. Independently of the initial conditions, whether uniform or centrally condensed, the matter develops a density distribution of the type $\rho \propto r^{-2}$, where r is the radial distance from the cloud center. In a time slightly longer than the free-fall time, the structure of the cloud is characterized

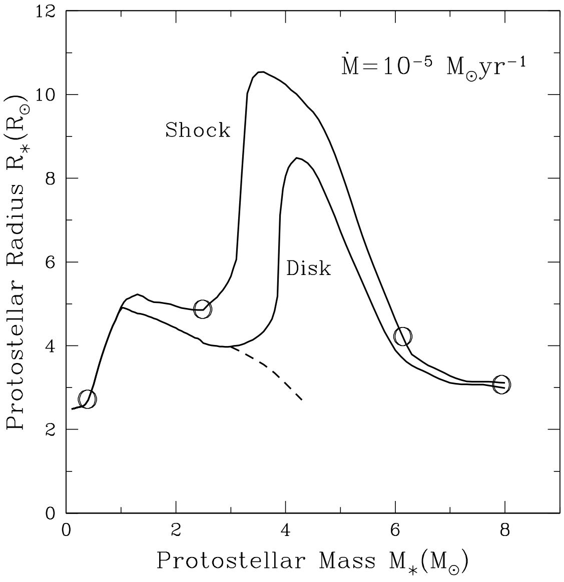

Figure 1. The evolution of the radius *vs.* mass in accreting protostars. The two curves refer to shock and disk accretion at a rate $\dot{M}$ =10^{-5} M$_\odot$ yr^{-1}. The open circles represent, from left to right, the ignition of central deuterium; the start of D-shell burning; the ignition of central hydrogen burning via the CN-cycle; the final arrival on the ZAMS. To gauge the importance of D-shell burning, the dashed curve shows the mass-radius relation obtained ignoring it in the case of disk accretion (adapted from Palla & Stahler 1991).

by the presence at the center of a stable hydrostatic core, which contains only few percent of the total cloud mass, accreting mass at the typical rate $\dot{M}_{\rm acc}$ (Stahler et al. 1980; Winkler & Newman 1980). At some point early in its growth, the hydrostatic core achieves central temperatures sufficient to ignite *deuterium burning* ($T_{\rm c} \sim 10^6$ K). The exact value of the core mass when this occurs depends on the magnitude of the accretion rate. For a value $\dot{M}$ =10^{-5} M$_\odot$ yr^{-1}, the ignition of deuterium starts at $M_* \sim 0.3$ M$_\odot$. The resulting mass-radius relations for protostars accreting at such a rate is shown in Figure 1 (Stahler 1988; Palla & Stahler 1990). The two curves refer to the evolution computed assuming that matter is accreted directly onto the protostar through a strong shock and to the case where the core surface is treated as a normal photosphere, as in the case of accretion through a circumstellar disk. Apart from minor quantitative differences, the *qualitative* behavior is similar, suggesting that it does not depend on the details of the accretion process.

The large radii predicted by Hayashi (see eq. 3) are never achieved. On the contrary, the protostellar radius remains limited to a few solar radii by the efficient radiation losses at the accretion shock. Note also that any value of $\dot{M}_{\rm acc}$ below that used in Fig. 1 would yield even smaller radii. In order to reproduce the Hayashi initial conditions, $\dot{M}_{\rm acc}$ should increase by more than two orders of magnitude. The evolution of the radius shown in Fig. 1 is the result of the nuclear burning of interstellar deuterium (D) in the accreting protostellar core. The general evolution can be separated into three main stages.

- $0.1 \lesssim M_*/M_\odot \lesssim 1$: for low-mass protostars, deuterium burning occurs near the center for temperatures exceeding $\sim 10^6$ K. The energy input is sufficient to turn and maintain the star convectively unstable. As more mass is gathered, the newly accreted deuterium is instantly transported by convective eddies to the center, and a situation of steady-state burning is created. In this condition, the deuterium generated luminosity, $L_{\rm D}$, is given by

$$L_D = \dot{M}_{\rm acc}\delta = 12L_\odot \left(\frac{\dot{M}_{\rm acc}}{10^{-5}M_\odot yr^{-1}}\right) , \tag{7}$$

where δ is the nuclear energy per unit mass available in interstellar matter (assuming a [D/H] value of 2×10^{-5} by number). The extreme temperature sensitivity of the energy generation rate is such that deuterium acts as an effective thermostat, preventing the central temperature from rising above $\sim 10^6$ K as the star gains mass. Since the amount of energy available in deuterium, δ, is comparable to the gravitational binding energy of the star, GM_*/R_*, the thermostatic effect results in a core radius that increases almost linearly with mass during the phase of active burning, as shown in Fig. 1 for $0.3 \lesssim M_*/M_\odot \lesssim 1$.

- $1 \lesssim M_*/M_\odot \lesssim 4$: the evolution of protostars more massive than solar is marked by the return of radiative stability and the onset of gravitational contraction. These events occur at about the same time, when the the deuterium generated luminosity, $L_{\rm D}$, is equal to the radiative luminosity, $L_{\rm rad}$. This condition is satisfied when

$$t_{\rm KH} \equiv \frac{GM_*^2}{R_*L_{\rm rad}} \approx \frac{GM_*^2}{R_*L_{\rm D}} \approx \frac{GM_*^2}{R_*\dot{M}\delta} \approx \frac{M_*}{\dot{M}} \equiv t_{\rm acc} \tag{8}$$

Eq. (8) establishes that the star is losing heat by radiation at the same time as it accretes new matter, and therefore it undergoes a phase of rapid gravitational contraction. Note that for low-mass stars, the accretion time is always much shorter than $t_{\rm KH}$. Because of the sensitivity of $L_{\rm rad}$ on M_* (see eq. 5), the equality of the two time scales is confined to a rather narrow range of masses, between 2 and 3 $M_\odot$. If nothing else happened in the interior, the rapid contraction would lead to the conditions appropriate for hydrogen burning in the center, and the star would then join the main-sequence while still accreting (as indicated by the dashed line in Fig. 1).

As a consequence, there should be no stars of mass greater than $2-3\ M_{\odot}$ in the PMS phase (e.g. Larson 1972). This result is in clear contradiction with the observational evidence of the Herbig Ae/Be stars, whose location in the H-R diagram is well above the ZAMS. The reason why this expected behavior does not occur is subtle, and is again related to the effects of deuterium burning.

When the thermodynamical conditions are appropriate, deuterium once more ignites, this time in a convective shell located at the transition between the inner radiative core and the external convective regions. This shell slowly shrinks toward the surface, due to the overall tendency of the star to become more and more radiatively stable. The release of nuclear energy in the lower density subsurface regions results in a dramatic swelling of the star, that doubles its radius. This is shown in the steep, almost vertical rise of the curve in Fig. 1. The expansion of the radius counteracts the gravitational pull, and retards the beginning of the phase of gravitational contraction.

- $4 \lesssim M_*/M_{\odot} \lesssim 8$: for more massive cores, the strength of the gravitational pull prevents a further increase of the radius, and the rapid expansion is replaced by a slow gravitational settling to the conditions of relaxed cores. Because of the swelling of the core, the interior temperature remains quite low, so that the approach to the ZAMS is naturally postponed to more massive cores. As shown in Fig. 1, central hydrogen burning is delayed until $\mathrm{M}_* \sim 6\ \mathrm{M}_{\odot}$, but the ZAMS is actually reached only at $\mathrm{M}_* \sim 8\ \mathrm{M}_{\odot}$. This finding reconciles the theoretical predictions of the protostellar models with observations of intermediate-mass PMS stars.

1.3. THE STELLAR BIRTHLINE

Under the assumption that protostars end their accretion phase in a time much shorter than t_{KH}, the mass-radius relation shown in Fig. 1 can be used to construct a theoretical *birthline* for stars of low- and intermediate-mass in the H-R diagram. The birthline is the locus along which young objects first appear as optically visible stars (Stahler 1983; Palla & Stahler 1990). Accordingly, there should be no observed PMS star whose position in the H-R diagram is *above* the birthline, since the largest radius a PMS star of a given mass can achieve is the protostellar radius at that mass. The resulting birthline is shown in Figure 2, together with the location of known T Tauri stars and Herbig Ae/Be stars. It is evident that the upper envelope of the stellar distribution is well matched by the theoretical birthline. The agreement also suggests that the specialized assumptions of the calculations (geometry, constant mass accretion rate) are not essential to the outcome of the mass-radius relation. Variations of the mass accretion rate induce a

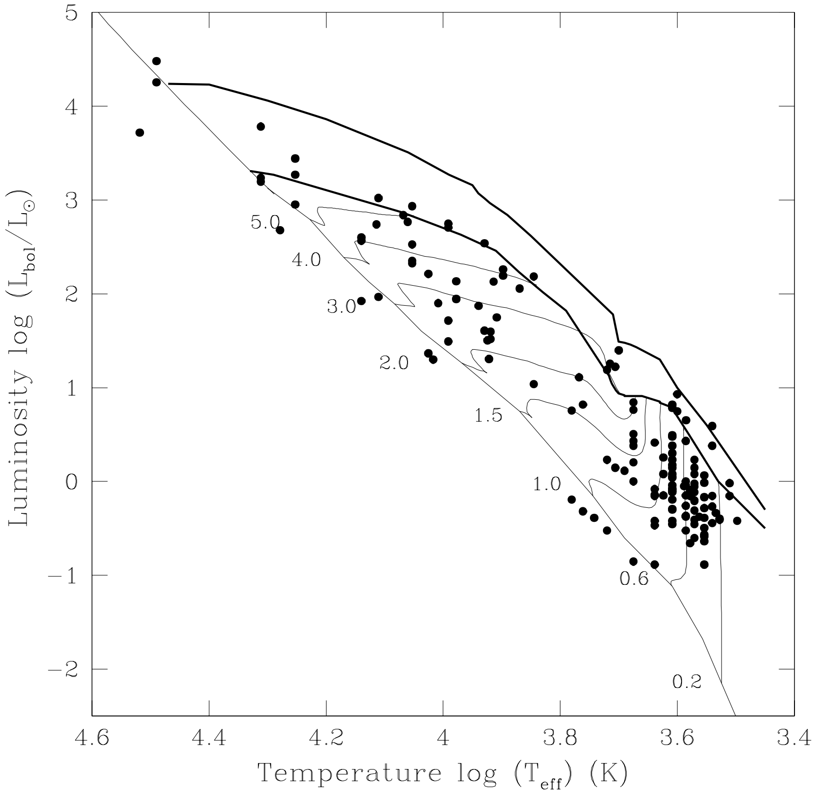

Figure 2. Location of the stellar birthline in the H-R diagram for accretion rates of 10^{-5} (*lower curve*) and 10^{-4} M$_\odot$ yr^{-1} (*upper curve*). Symbols give the position of young PMS stars. Labeled curves are PMS evolutionary tracks for the indicated stellar mass. The location of the ZAMS is also indicated (adapted from Palla & Stahler 1993).

change in the mass-radius relation: for higher $\dot{M}_{\rm acc}$, the various evolutionary phases described above remain unaltered, even though each event is shifted to higher masses. The resulting birthline shown in Fig. 2 by the upper curve for $\dot{M}_{\rm acc} = 10^{-4}$ M$_\odot$ yr^{-1} does not improve significantly the agreement with the observational data. These considerations lead to the conclusion that an accretion rate $\dot{M}_{\rm acc} \sim 10^{-5}$ M$_\odot$ yr^{-1} can represent the typical value for the formation of stars in a mass range from few tenths of a solar mass to about 10 M$_\odot$.

2. Pre–main-sequence evolution

Once the main phase of accretion is completed, the stellar core emerges as an optically visible star along the birthline. The physical process by which infall stops is still not known, although stellar winds and bipolar outflows must play a fundamental role. The circumstellar matter surrounding these young stars, partly distributed in a disk and the rest in an extended envelope, still emits copiously at infrared wavelengths: the emergent spectral energy distribution departs substantially from that of a normal stellar photosphere, showing excess emission extending from the near- to the far-infrared. The origin of this excess has been commonly attributed to the presence of accretion disks. Depending on the mass of the star, young visible stars are classified as T Tauri (low-mass, typically $\sim$1 $M_\odot$), or Herbig Ae/Be stars (intermediate-mass, $\lesssim$10 $M_\odot$). Their early evolution can be followed in detail, once the initial conditions for the gravitational contraction phase toward the Main Sequence are specified. The birthline joins the ZAMS at $M_* \sim 8$ $M_\odot$. Thus, for stars with masses above this value there is no optical PMS phase: the rapid gravitational contraction in these objects has led to hydrogen ignition already during the accretion phase. Massive stars are born *on* the ZAMS. In this section, the basic features of theoretical models of PMS evolution will be outlined.

2.1. PROTOSTELLAR INITIAL CONDITIONS

The results of protostellar evolution described in Section 2 show that the classical assumptions are no longer appropriate. First, protostellar cores never reach large radii: the radius remains typically a factor of ten smaller than that predicted by eq. (3). It is reasonable to assume that the protostellar radii represent the *maximum* values that a star of a given mass can achieve prior to contraction. Second, the internal structure departs significantly, at least for intermediate-mass objects, from the assumption of thermal convection. In low-mass stars, convection is due to central nuclear burning. Protostars more massive about 2 $M_\odot$ are radiatively stable in the inner regions, and possess a thick, subsurface mantle of deuterium. This deuterium must ignite in a shell to fuse to helium during the approach to the main sequence. The disparate state of the two regions implies that the stars are *thermally unrelaxed* at the beginning of the PMS evolution. Thus, in contrast to the situation described by the classical theory, these stars must undergo *non-homologous* quasi-static contraction (Palla & Stahler 1993).

Another important aspect is that for a PMS of fixed mass, the amount of deuterium available is that which a protostar of the same mass did acquire in the course of its accretion history. The variation of the fractional deuterium concentration, $f_{\rm D}$, for a protostar accreting at different rates is shown in Figure 3. Here, $f_{\rm D}$ is calculated relative to the interstellar concentration. We see that for the lowest values of the accretion rate $f_{\rm D}$ declines

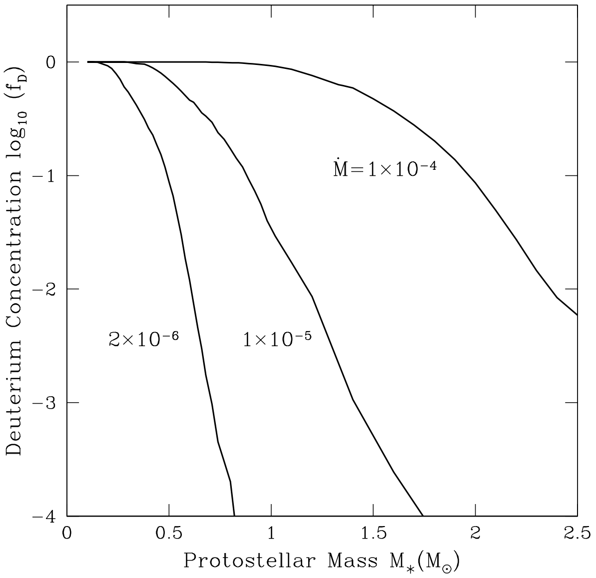

Figure 3. Evolution of the fractional deuterium concentration, f_{D}, in protostars accreting at different values of the accretion rate.

quite rapidly for $\mathrm{M}_* \lesssim 1\ \mathrm{M}_\odot$, even thoguh the star is fully convective, and therefore accreting deuterium as fast as it is being consumed. Actually, consumption slightly exceeds accretion, and L_{D} differs correspondingly from the value in equation (7). The evolution of f_{D} in a fully convective protostar is given by

$$M_* \frac{df_D}{dM_*} = 1 - f_D - \frac{L_D}{\dot{M}\delta} \ , \tag{9}$$

from which it follows that

$$L_D = \dot{M}\delta \left[1 - \frac{d(f_D M_*)}{dM_*} \right] \ . \tag{10}$$

Since the product $f_{\mathrm{D}} M_*$ is proportional to the total deuterium content, equation (10) shows that any net loss of deuterium implies that L_{D} exceeds $\dot{M}_{\mathrm{acc}}\delta$. Such loss is inevitable, because of the slowly rising interior temperature of the protostar. The fall of f_{D} shown in Fig. 3 continues until the radiative barries appears, and thereafer deuterium exists only in a small, subsurface mantle. For fast accretion rates, the drop of deuterium in the protostellar phase is postponed at masses $\mathrm{M}_* \sim 1.5\ \mathrm{M}_\odot$.

2.2. STELLAR STRUCTURE EQUATIONS

Unlike the previous hydrodynamical protostellar phase, the PMS evolution of a star can be followed by models in hydrostatic and thermal equilibrium. These models are much easier to construct and less subject to numerical inaccuracies. The subject of stellar structure equations is well established and fully described in numerous textbooks. Here, I will present a brief description of the main equations needed for the calculation of PMS stellar models.

The *mechanical* stellar structure equations are simply a restatement of hydrostatic balance. If we neglect internal rotation, then a convenient spatial variable in a spherical star is the mass coordinate $M_{\rm r}$, defined by

$$M_r \equiv \int_0^t 4\pi r^2 \rho dr \ , \tag{11}$$

where ρ is the mass density of the gas. The function $M_{\rm r}$ represents the mass enclosed within a sphere of radius r. From equation (11) we have immediately $\frac{dM_r}{dr} = 4\pi r^2 \rho$. The radius r then acts as a dependent variable, whose variation with M_r is governed by the inversion of this expression

$$\frac{dr}{dM_r} = \frac{1}{4\,\pi\, r^2\, \rho} \ . \tag{12}$$

The internal pressure is related to the total weight by

$$\frac{dP}{dr} = -\frac{G\,\rho\, M_r}{r^2} \ . \tag{13}$$

Dividing (12) by (13) we derive the alternate form

$$\frac{dP}{dM_r} = -\frac{G\,M_r}{4\,\pi\, r^4} \ , \tag{14}$$

which again utilizes M_r as the independent variable. The pressure itself obeys the equation of state for an ideal gas:

$$P = \frac{\rho}{\mu} \mathcal{R}\, T \ . \tag{15}$$

Here the mean molecular weight μ depends on the state of ionization and dissociation of the gas, and is therefore a function of ρ and T. One may either calculate this function *ab initio*, by invoking statistical equilibrium, or obtain it from prior tabulations.

We turn next to the *thermal* stellar structure equations. Since the protostar's interior is highly opaque, the transport of radiation is governed by the diffusion equation

$$T^3\, \frac{dT}{dM_r} = -\frac{3\,\kappa\, L_{\rm int}}{256\,\pi^2\,\sigma_B\, r^4} \ . \tag{16}$$

The Rosseland mean opacity κ is again a function of ρ and T. Like μ, it is available in numerical form.

Finally, we consider the spatial variation of $L_{\rm int}$. Recall that the latter is the surface integral over a spherical shell of $|F_{\rm rad}|$, where the flux points radially outward. In general, a fluid element gains heat either by being irradiated externally or from internal nuclear reactions. Let $\epsilon\,(\rho, T)$ represent the rate of nuclear energy release per unit mass. Both this rate and $F_{\rm rad}$ enter as source terms in the *heat equation*:

$$\rho T \,\frac{ds}{dt} \,=\, \rho\epsilon \,-\, \nabla\cdot F_{\rm rad} \ , \tag{17}$$

where s is the entropy per unit mass of the fluid. For a spherical star, it is convenient to recast this relation as

$$\frac{dL_{\rm int}}{dM_r} \,=\, \epsilon \,-\, T\,\frac{ds}{dt} \ . \tag{18}$$

Equations (12), (14), (16), and (18) are the desired stellar structure equations for the dependent variables r, P, T, and $L_{\rm int}$. They must be supplemented by the equation of state (15) and by knowledge of μ, κ, ϵ, and s as functions of ρ and T. In practice, tabulations of the entropy utilize the Second Law of thermodynamics:

$$T\,\Delta s \,=\, c_v\,\Delta T \,-\, P\,\Delta\rho/\rho^2 \ , \tag{19}$$

which governs small changes of the state variables. Here, c_v is the specific heat at constant volume. Knowing this latter quantity (or, equivalently, the specific internal energy) as a function of ρ and T allows one to integrate equation (19) in the $\rho - T$ plane and numerically obtain the function $s(\rho, T)$. Note that a purely monatomic gas would have $c_v = (3/2)\mathcal{R}/\mu$, where μ is now a constant. In this case, we may integrate equation (19) analytically to obtain

$$s \,=\, \frac{\mathcal{R}}{\mu}\,\ln\!\left(\frac{T^{3/2}}{\rho}\right) \,+\, s_\circ \ , \tag{20}$$

where $s_\circ$ is an arbitrary constant. Equation (20) is often a useful approximation in stellar interiors, where the gas is fully ionized and $\mu = 0.61$.

Solution of the stellar structure equations requires specification of four boundary conditions. Two of these are the statements that both $r\,(M_r)$ and $L_{\rm int}\,(M_r)$ vanish at the center of the configuration:

$$M = 0: \quad r\,(0) \,=\, 0 \quad L_{\rm int}\,(0) \,=\, 0 \ . \tag{21}$$

A third condition is that $P\,(M_r)$ must equal the appropriate photospheric value when $M_r = M_*$:

$$M = M_* : \quad P_{\rm e} \;=\; \frac{2}{3}\frac{GM_*}{R_*^2\kappa} \;. \tag{22}$$

The fourth boundary condition concerns the surface value of the temperature and its relation to the luminosity. For a PMS star, this relation is the standard photospheric one given by equation (4):

$$M = M_* : \quad L \;=\; 4\pi R_*^2 \sigma T_{\rm eff}^4 \;. \tag{23}$$

The full four stellar structure equations can now be solved as a two-point boundary value problem, in which the values of the pressure and entropy are guessed at the center, while the stellar radius and luminosity are guessed at the surface. One can integrate the equations from both directions to an interior fitting point, where the four guesses must be changed until all variables match.

2.3. INPUT PHYSICS

The four basic ingredientes required by the stellar models are the equation of state, opacity, treatment of convection and the nuclear generation rate. Each of these physical processes would require a lengthy discussion, which is beyond the scope of this chapter. I will confine myself to a brief summary of some basic aspects and refer the reader to general reviews for more information.

2.3.1. *Equation of state*

The importance of using a good equation of state (EOS) for stellar models has been discussed by Däppen (1993) and by D'Antona (1993) for the case of PMS stars. The task is to develop a formalism for the computation of the EOS valid from the conditions of the photosphere, where the temperature is typically a few 10^3 K and the density some 10^{-7} g cm^{-3}, to the center of a star where $T\ \sim\!10^7$ K and $\rho\ \sim\!10^2$ g cm^{-3}. In the first approximation, PMS stars, because of contraction and of the relatively low density, should behave according to the ideal gas law. However, the Saha formula is just an approximation that no longer holds as soon as a small degree of degeneracy or other non-ideal gas effects are present. Mazzitelli (1989) has discussed in detail the implications of including non-ideal gas effects on the hydrogen and helium ionization. An important result is that because of the decrease of the value of the adiabatic gradient in regions of partial ionization, stellar models are charactized by *lower* effective temperatures The most recent efforts to derive reliable EOS for astrophysical use include

Mihalas, Hummer & Däppen (1988), as part of the international "Opacity Project" (OP), and Iglesias & Rogers (1991), as part of the opacity project at Livermore (OPAL). A clear explanation of the physical approach behind the two computations and comparisons between the results are presented by Däppen (1993).

2.3.2. *Opacity*

There has been a dramatic improvement in the calculation of the Rosseland mean opacity of gas mixtures over the last ten years. Prior to 1990, the only existing set of opacities were provided by the Los Alamos group, both at high ($T>10^4$ K) and low-temperatures ($T<10^4$ K) (Huebner et al. 1977; Cox & Tabor 1976). In the latter regime, an important contribution has been done by Alexander and collaborators who considered the presence of molecules and grains in the computations (Alexander et al. 1989; Alexander & Ferguson 1994). The physical processes considered in the calculations include continuum sources of opacity due to 14 elements (H, H^-, H_2^+, H_2^-, He, plus heavy elements); atomic and molecular lines (about 60 million transitions); electronic and Rayleigh scattering due to H, H_2 and He; absorption and scattering of grains with radius between 0.005 and 0.25 μm.

At temperatures above 8000 K, both the OPAL and OP projects provide extended tabulations of the opacity, including free-free, bound-bound and bound-free transitions for many elements from hydrogen to iron. The motivation for these calculations is interesting. In 1982, Simon made a plea for the re-examination of the heavy element contribution to opacities. He showed that an increase in the contributions from elements heavier than helium by factors of two or three in envelope regions, would resolve a number of outstanding problems in the theory of pulsating stars. Two groups, OPAL and OP, responded to the plea and performed calculations that showed that indeed a better treatment of atomic physics led to significant opacity enhancements that helped to solve the problem of Cepheid pulsation (Iglesias & Rogers 1991; see also Seaton 1993 for a review). The opacity tables are constantly updated, as improvements in atomic physics are obtained (Rogers & Iglesias 1992; Iglesias & Rogers 1996; Seaton et al. 1994). As an illustration of the properties of the Rosseland mean opacity at selected densities, Figure 4 shows the behavior of the opacity at low- and high-temperatures for different sets of tables. In the right panel, the peak at $T\sim10^5$ K, called the *Z-bump*, visualizes the impact of the OPAL calculations on the behavior of the opacity in the inner regions. This feature stems from bound-bound transitions involving the inner electrons of heavier metals, principally iron. The main peak at $T\sim10^4$ K is due to the photoionization of hydrogen. At lower temperatures, the opacity falls

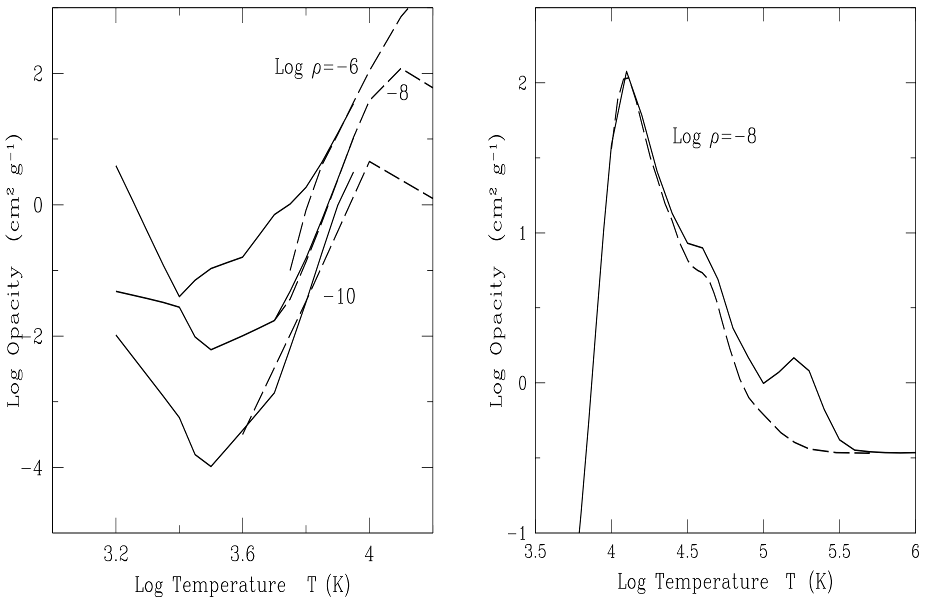

Figure 4. Rosseland mean opacities for a gas of solar composition. *Left panel*: comparison of the low-temperature opacities for different densities. The solid lines are from Alexander et al. (1994) and the dashed lines from Rogers & Iglesias (1992). Note that the latter do *not* include the contributions from molecules. *Right panel*: high-temperature opacities for a density of 10^{-8} g cm^{-3}. Solid line is from Rogers & Iglesias (1992) and the dashed line is from Cox & Tabor (1976). Note the enhancement of the opacity at T$\sim 10^5$ K (*Z-bump*).

steeply because too few photons in the Planckian distribution have energies exceeding the ionization threshold of 13.6 eV. The decline in opacity with falling temperatures halts temporarily at near 2000 K, where the dominant process is now bound-bound transitions in molecules (left panel).

Molecules play a dominant role in the atmospheres of cool dwarfs, from mid K to late M stars and a mass from 0.6 $M_\odot$, to the hydrogen burning limit (0.075-0.085 $M_\odot$, depending on metallicity), and in the brown dwarf regime. In such stars, most of the hydrogen is locked in H_2 and most of the carbon in CO, with excess oxygen bound in molecules such as TiO, VO, and H_2O (e.g. Allard et al. 1997). These molecules can serve as useful diagnostics of the nature of the very low-mass stars. Opacities due to grains are also becoming available (e.g. Alexander et al. 1998). Grains can condensate in stellar atmospheres at temperatures below ∼2000 K, and their effect is to decrease the gas phase abundance of some important absorbers, such as TiO. The impact of grain opacity on the spectral distribution and atmosphere of cool stars is quite important, but a full understanding of the physics of grain condensation and absorption is still lacking.

2.3.3. *Treatment of convection*

The standard treatment of turbulent convection is a phenomenological one, based on Prandtl's theory of turbulence with the introduction of a quantity called the *mixing length* (Böhm-Vitense 1958). Despite its limitations, the mixing length theory (MLT) gives a satisfactory description of the convective zone since this region is to a large extent very close to being adiabatic. In the MLT theory, the length l over which a convective bubble merges with its surroundings is assumed to be proportional to the pressure scale height $H_{\rm P}$, $l = \alpha H_{\rm P}$, where α is a free parameter and $H_{\rm P} = -dr/dlnP$. The actual value of α is chosen as to fit the solar radius and effective temperature. In general, α=1.5 yields a good fit. However, the surface properties of stellar models are quite sensitive to the value of α adopted in the computations. Lowering (rising) α to 1 (2) instead of 1.5 reduces (increases) the values of the effective temperature by about 10% (i.e. several hundred degrees), especially along the Hayashi vertical track (e.g. Forestini 1994). Thus, the poor knowledge of stellar convection introduces considerbale uncertainties in the location of the tracks in the H-R diagram. Also, the temperature at the base of the convection zone is very sensitive to the value of α. Therefore, important differences in the level of light elements depletion in the convective envelopes result from different choices of the mixing length parameter.

An alternative theory to the MLT has been presented by Canuto & Mazzitelli (1991, CM) and Canuto, Goldman & Mazzitelli (1996). Unlike MLT which considers a single element of turbulence ("one-eddy" description), the CM convection model takes into account the full spectrum of the eddy distribution. Also, the mixing length is chosen to be the harmonic mean between the distance z of the layer from the top and the distance from the bottom of the convective region. The properties of the Sun can then be fitted to high precision (less than 1%, as demanded by heliosismological constraints) by introducing a small amount of overshooting from the surface convective layer and the prescription for the scale lenght becomes $l = z + \beta H_{\rm P}$. A full description of the CM convection model, together with a discussion on the reasons to adopt such a model instead of the MLT, can be found in the review by D'Antona & Mazzitelli (1998).

2.3.4. *Nuclear reactions*

The nucleosynthesis during the PMS phase is limited to the light elements. In addition to the destruction of deuterium, the nuclear burning of ^{6}Li, ^{7}Li, ^{9}Be, and ^{3}He takes place when the central temperature in solar-type stars reaches values of 2×10^6 K, 3×10^6 K, 3.5×10^6 K, and 8×10^6 K. However, the relatively tiny abundances of these species render the effect energetically and structurally unimportant. For example, the interstellar lithium abundance is [Li/H]$\sim 10^{-9}$: in order to halt PMS contraction, the abundance should be enhanced by a factor 10^5 or more over the observed ones. On the other hand, the depletion history of lithium in low-mass stars can be followed in detail to compare with observations and to test the internal structure of stars.

The nuclear network consists of the complete *pp* chain and the CNO cycle. Deuterium and ^{7}Li burning are considered separately, since they occur before the *pp* chain takes over. The computation of the energy generation requires the knowledge of the nuclear cross sections. These are tabulated by Caughlan & Fowler (1988), while weak and intermediate screening factors can be computed using the formalism of Graboske et al. (1973). Screening is also important for D and ^{7}Li burning reactions, especially for very low-mass stars and brown dwarfs. The relative concentration of the nuclear species follows the solar composition (e.g. Anders & Grevesse 1989) with a metal abundance Z=0.019. The location of PMS tracks is not sensitive to the exact value of the metallicity; however, the amount of ^{7}Li depletion is strongly affected by Z, increasing for larger values of Z (D'Antona & Mazzitelli 1984).

3. A new H-R diagram

The results of the calculations of PMS evolution incorporating the protostellar initial conditions and the input physics discussed in Section 3 are shown in the H-R diagram of Figure 5 for stars from 0.1 to 6.0 $M_\odot$ (Palla & Stahler 1999). The evolutionary tracks have been computed using the opacities of Alexander et al. (1994) at T<8000 K and of Rogers & Iglesias (1992) at higher temperatures. Convection has been treated using MLT with α=1.5. From Fig. 5, we can see that while low-mass stars descend from the birthline on convective paths, stars more massive than $\sim$4 $M_\odot$ move to the left on radiative ones. Stars between 2 and 4 $M_\odot$ undergo thermal relaxation, looping back slightly behind the birthline and recrossing it before pursuing horizontal tracks. Compared to the classical set of PMS tracks, those shown in Fig. 5 occupy a much more limited portion of the diagram. The reason is that the older tracks correspond to stellar radii too large to have attained during protostellar accretion. Thus, the starting luminosities are much lower than previously envisioned. In addition, the surface temperature of these stars begin *higher*. For example, a 5 $M_\odot$ star starts with $T_{\rm eff}$=12000 K in contrast to the value of 4400 K obtained by Iben (1965). Notice also that the birthline intersects the main sequence at a mass $M_* \sim 8$ $M_\odot$: this point represents the critical stellar configuration in which hydrogen burning has stopped gravitational contraction while the star is still growing in mass (see Fig. 1). *More massive stars, therefore, have no PMS phase at all, but appear directly on the main sequence once they are optically revealed.*

An important result of the new calculations is that observed PMS stars should not be located to the right of the birthline. For both T Tauri and Herbig Ae/Be stars the agreement is excellent, despite the rather strong assumption of a constant mass accretion rate of 10^{-5} $M_\odot$ yr^{-1} used in the models (see Fig. 2). This fact indicates that a limited dispersion in the properties of molecular cloud cores (which determine the magnitude of $\dot{M}_{\rm acc}$) somehow produces an impressive range of stellar masses. The case for even more massive stars is complicated by the difficulty in determining the appropriate stellar parameters to place them in the H-R diagram

Finally, another important result is the drastic reduction in age obtained for Herbig Ae/Be stars. The same is true, of course, for T Tauri stars, but the quantitative impact is minor. Even a large drop in the initial radius of a typical T Tauri star hardly changes its total contraction age, since $t_{\rm KH}$ scales as R_*^{-3}. For the Herbig stars, however, equation (8) implies that $t_{\rm KH}$ only increases as $R_*^{-1/2}$. The age reduction is far more significant for masses well below the upper cutoff at 8 $M_\odot$. Such a reduction is consistent with the observations of surface activity in these stars.

3.1. LOW-MASS STARS: $0.1 \lesssim M_*/M_\odot \lesssim 1$

The largest departure from the standard theory of PMS stars concerns the history of deuterium burning. Salpeter (1954) was the first to recognize that deuterium ignition via the reaction ^{2}H(p,γ)^{3}He at a temperature of about 1×10^6 K could slow down contraction or, for the least massive stars, stops it entirely for a relatively brief time. This effect was confirmed by the detailed calculations of Grossman & Graboske (1971) and Mazzitelli & Moretti (1980) who introduced the concept of a "deuterium main sequence" to denote the curve in the H-R diagram crossed by the PMS tracks at the point of ignition. However, Stahler (1988a) has shown that this concept is obsolete, since deuterium burning occurs already during the accretion phase for stars with masses above a few tenths of a solar mass (see Fig. 3). Thus, the locus of the deuterium main-sequence is nothing else than the birthline shown in Fig. 5. T Tauri stars, having consummed most of the available deuterium during the accretion phase, begin the contraction phase by simply descending along the vertical portion of the Hayashi track. The same is true for a Herbig Ae/Be star, which begins with a severely depleted deuterium supply. While this supply lasts, the outermost layers remain convectively unstable. But the luminosity provided by deuterium burning

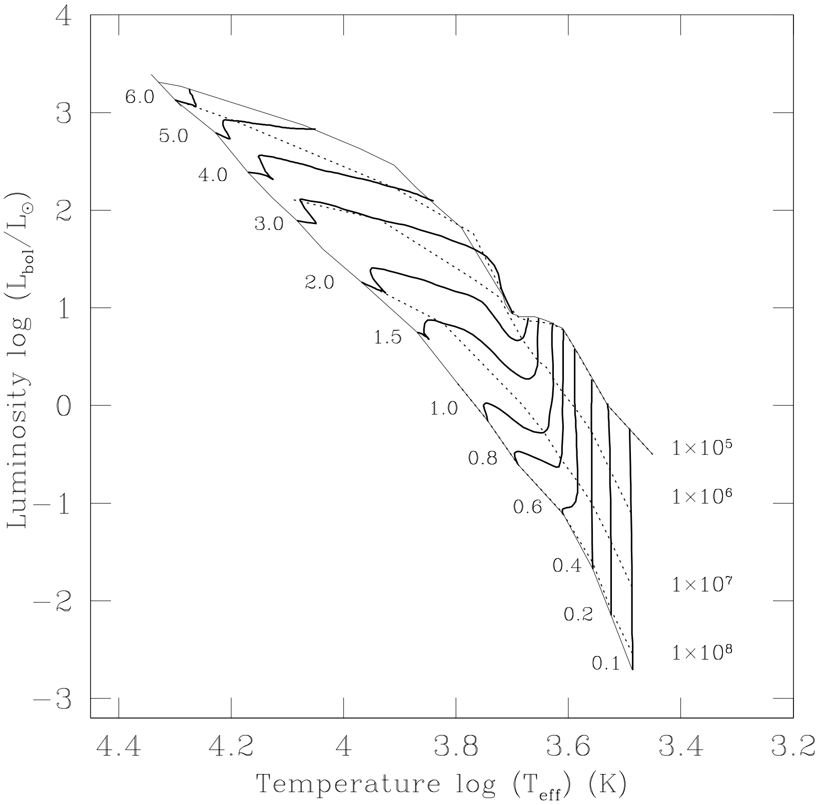

Figure 5. Evolutionary tracks in the H-R diagram for low- and intermediate-mass stars. Each track is labeled by the corresponding mass, in solar units. Selected isochrones are shown by the dotted lines. For each track, the evolution starts at the birthline (dotted curve), and ends at the ZAMS, also shown (from Palla & Stahler 1998).

$L_{\rm D}$ is now so minor compared to $L_{\rm rad}$ that even this limited convection vanishes by the time the star has joined the classical radiative portion of its evolutionary track. Finally, for stars of mass smaller than $\sim$0.3 $M_\odot$, protostar theory still implies deuterium burning during the PMS phase, while for masses as low as M_*=0.018 $M_\odot$ degeneracy effects set in and prevent nuclear burning (D'Antona & Mazzitelli 1994).

3.2. INTERMEDIATE-MASS STARS: $1 \lesssim M_*/M_\odot \lesssim 8$

For stars more massive than solar, the imprint of the prior accretion history persists much longer than in the low-mass, convective case. The reason is that the stellar interior is not thermally relaxed, and the stars must undergo a phase of global readjustment. The main results can be schematically summarized as follows.

- *Fully convective stars*: Stars in the range $1 - 2.5\ M_{\odot}$ are fully convective due to surface cooling as soon as they appear as optically visible objects. The evolution is undisturbed by the fusion of residual deuterium: its concentration is so low, that it is quickly consumed (on a time scale of few years). Stars contract along the Hayashi track, but their path is much reduced (see the case for $M_* = 2\ M_{\odot}$ in Fig. 5).

- *Partially convective stars*: Stars in the range $2.5 - 4\ M_{\odot}$ undergo thermal relaxation and nonhomologous contraction. When they are first optically visible, they are *underluminous*: i.e., the evolutionary track begins at low luminosity and then moves up to join the radiative portion. The Hayashi phase is skipped entirely. In the H-R diagram, shown in Figure 6 for the case of a 3.5 $\mathrm{M}_{\odot}$ star, the unrelaxed star first appears below the classical evolutionary track for that mass. At this early epoch, the star has a relatively shallow convection zone. During subsequent relaxation, the stellar radius, surface luminosity and temperature all increase, while the outer convection disappears. The variation of the distribution of the internal luminosity at different times is also shown in Fig. 6. Initially, the function $L_{\mathrm{r}}(M_{\mathrm{r}})$, the luminosity crossing any interior shell enclosing a mass M_{r}, rises from zero at the center, peaks somewhere in the interior, then falls again to the relatively low surface values L_{surf}. Such odd luminosity profile cannot be maintained indefinetely. According to the heat equation (18), matter between the star's center and the shell where L_{r} peaks is losing heat ($ds/dt < 0$), while the gas between this shell and the surface is gaining heat. As shown in Fig. 6, this internal heat transfer, achieved entirely through radiative diffusion, causes the peak of L_{r} to move outward with an attendant rise in the surface luminosity. The approximate duration of this *thermal relaxation* is given by the Kelvin-Helmoltz time with L_{surf} replaced by the internal luminosity L_{rad} in equation (5).

The luminosity in stars of mass between $2.5 - 4\ M_{\odot}$ stems almost entirely from gravitational contraction. This contraction, however, is initially quite different from that envisioned in the classical PMS theory. That interior portion which is losing heat indeed shrinks, but the transfer of this energy actually expands the outer region and creates a net increase of the stellar radius. This *nonhomologous contraction* continues until $L_{\mathrm{r}}(M_{\mathrm{r}})$ is everywhere increasing, by which point the star as a whole is shrinking, as in the classical model.

- *Fully radiative stars*: Stars more massive than $4\ M_{\odot}$ appear immediately on the radiative portion of the classical track, and begin to contract homologously under their own gravity. As the star contracts, the average interior luminosity must rise as $\mathrm{R}_*^{-1/2}$, according to equation (4). Such rise is evident in the evolutionary tracks of Fig. 5. The specific entropy decreases

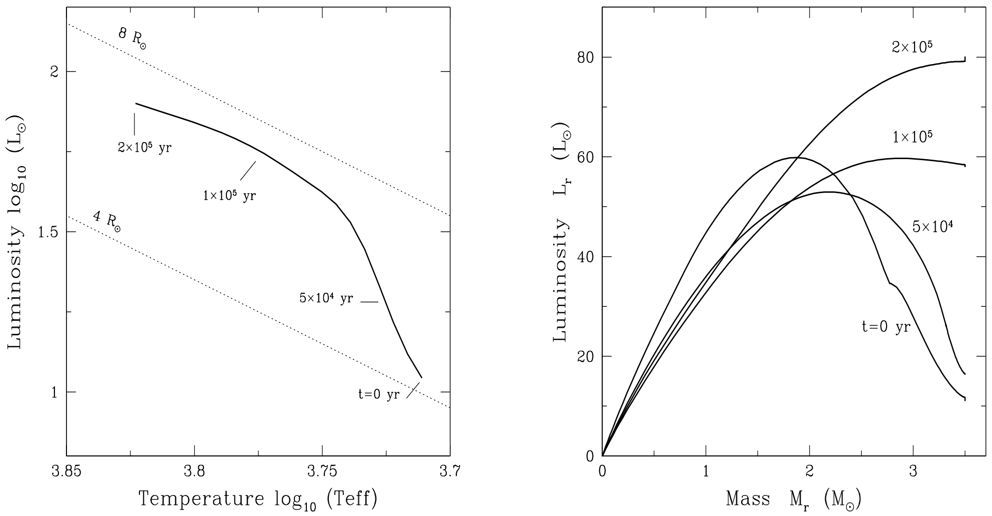

Figure 6. Left panel: Early evolution in the H-R diagram of a 3.5 $M_\odot$ star, covering the phase of thermal relaxation. The thin dashed lines are cruves of constant radius. Right panel: The evolution of the internal luminosity during the thermal relaxation process. Note the shift of the peak in luminosity toward the stellar surface as a result of nonhomologous contraction. (Adapted from Palla & Stahler 1993)

with time in all interior mass shells, a sign of homologous contraction. At any one time, the interior is radiative, i.e. the entropy is increasing outward, except for a very thin surface layer.

In comparison with standard Iben's calculations (1965), the new tracks shown in Fig. 5 occupy a much reduced portion of the H-R diagram. In addition, the surface temperatures are *higher*, since the outermost layers are fully ionized, and the dominant opacity source in this region is no longer the H^- ion. In conclusion, the combination of protostellar and PMS theory does seem to account for at least one basic property of T Tauri and Herbig Ae/Be stars: their distribution in the H-R diagram. As shown in Fig. 2, the upper envelope of the stellar distribution is well matched by the theoretical birthline obtained with the fiducial value of 10^{-5} $M_\odot \mathrm{yr}^{-1}$.

3.3. MASSIVE STARS: $\mathrm{M}_* \gtrsim 8$ $\mathrm{M}_\odot$

The process of gravitational contraction during the accretion phase ends when the nuclear luminosity due to the CNO cylce becomes dominant. There is no precise way to specify the arrival of a protostar at the main sequence, since the models are never identical to ZAMS stars of the same mass. For example, at M_*=8 $M_\odot$, the nuclear luminosity still accounts for 75% of the total luminosity, with the remainder provided by gravitational settling in the outer layers. However, we know that the stellar radius must reach a minimum if accretion were to increase indefinetely. From Fig. 1, the value of the minimum R_* is 3.1 $R_\odot$. This radius is reached on the theoretical ZAMS at $M_* \approx 8$ $M_\odot$ (Iben 1965). Thus, we may take this mass as the value where the protostar has joined the main sequence. The consequence is obvious: there is no longer any PMS phase for stars more massive than this value. They can only be observed as infrared accreting protostars or as main-sequence or post-main sequence objects.

An implication of the evolution described so far is that most stars should form with nearly the same accretion rate, as supported by the distribution of known PMS star in the H-R diagram. One possible objection to this hypothesis is that stars forming at modest rates might complete their entire main-sequence evolution *before* reaching a sufficiently high mass. However, with an $\dot{M}_{\rm acc}$ of 10^{-5} $M_\odot$ yr^{-1}, the accretion and nuclear lifetimes become equal only at a stellar mass of 45 $M_\odot$, while with $\dot{M}_{\rm acc}=10^{-4}$ $M_\odot$ yr^{-1} the critical mass is higher than 100 $M_\odot$ (Schaller et al. 1992). These figures suggest that even high-mass stars, i.e. those with no visible PMS phase, form with accretion rates in the range considered above and do not require extreme conditions. This possibility has been considered by Beech & Mitalas (1995) and Bernasconi & Maeder (1996) who studied the formation and evolution of stars up to $\sim$100 $M_\odot$ under the accretion scenario. One of the interesting findings is the definition of an upper stellar birthline as an extension above $\sim$10 $M_\odot$ of that shown in Figs. 2 and 5. A massive star then begins its main-sequence evolution from these initial conditions that differ substantially from those at the classical ZAMS. In particular, massive stars begin their evolution with lower effective temperatures and with a reduced extent of the convective core.

However, accretion cannot proceed indefinetely because of the mechanical effect of the protostar's radiation on the infalling envelope. The accretion shock at the stellar and disk surfaces produces photons at optical and ultraviolet wavelengths. These are absorbed by the envelope's dust grains and reradiated into the infrared. Trapping of this infrared radiation creates thermal pressure that retards infall. The stellar luminosity also raises the envelope's temperature until the grains sublimate at the dust destruction front. The direct impact of short-wavelength photons on grains at this front provides an additional retarding force. Radiation pressure begins to become significant in protostars of intermediate mass. Infall cannot be stopped, however, as long as the accretion component dominates the total luminosity. Any retardation of the flow diminishes $\dot{M}_{\rm acc}$, which in turn lowers L_*. Once the luminosity falls, the flow picks up again. Numerical simulations of collapsing clouds with central stars display this effect. For stars in the proper mass range, $\dot{M}_{\rm acc}$ oscillates strongly without actually reversing (Yorke and Krügel 1977). The feedback between radiation pressure and infall is cut once $L_{\rm int}$ dominates L_*. Again, the transition occurs just where $t_{\rm KH}$ falls below $t_{\rm acc}$, *i.e.*, for protostars that have joined the main sequence. The internal luminosity is now supplied by hydrogen fusion rather than contraction, but still scales as $M_*^{11/2} R_*^{-1/2}$. Hence the retarding force on the envelope increases rapidly with mass. Within the context of spherical collapse, the result is inevitable and the condition of balance between the forces yields

$$\frac{L_*}{M_*} = \frac{4\pi c G}{\kappa} = 1 \times 10^3 \frac{L_\odot}{M_\odot} \ , \tag{24}$$

where it has been used a value of κ=10 cm^2 g^{-1} for the opacity. Plausible variations in grain composition could alter this value by as much as a factor of 3 in either direction (Draine & Lee 1984; Pollack et al. 1994). Thus, the critical ratio occurs at a mass near 10 M$_\odot$, implying that accretion is significantly affected for central objects of greater mass. Wolfire and Cassinelli (1987) analyzed the dynamics of envelopes falling onto stars with M_* exceeding 60 $M_\odot$. They found that infall was reversed unless $\dot{M}_{\rm acc}$ were arbitrarily increased to *at least* 10^{-3} $M_\odot$ yr^{-1} *and* grains were depleted in abundance by an order of magnitude. Since these extreme conditions are unlikely to occur, we are faced with a basic dilemma. (For earlier discussion of this issue, see Larson and Starrfield 1971 and Kahn 1974.)

There is little doubt that a massive star produces more than enough energy to expel its envelope. In fact, the inequality $t_{\rm KH} < t_{\rm acc}$ implies that the radiated luminosity can easily unbind the parent cloud before the star has gained appreciable mass. The real issue is the *efficiency* of energy transfer. Here, any departure of the infall from spherical symmetry is likely to play a major role (Nakano 1989). Unfortunately, a consistent theory which includes rotation and the simulataneous presence of infall and outflow is still unavailable, so that the formation of massive stars via accretion remains a mistery. Perhaps, one should invoke a completely different scenario (e.g. collision/coalascence models in dense clusters; Bonnell, Bate & Zinnecker 1998; Stahler, Palla & Ho 1999).

4. Tests to PMS evolutionary diagrams

The location of young stars in the H-R diagram is commonly used to estimate their masses and approximate ages. When young clusters or associations are studied, the information on the mass of individual members can yield direct information on the rate and efficiency of star formation and, eventually, on the initial mass function to compare to that observed locally.

Also, the amount of depletion of the light elements due to nuclear activity in these early stages sheds light on the internal structure and on the mechanisms of angular momentum transport. It is important at this point to discuss the uncertainties that affect the computation of modern evolutionary tracks, such as those described earlier. The sources of uncertainty can be due to the uncertain knowledge of certain aspects of the input physics used in the theoretical models, or to the complex phenomena that accompany the evolution of young stars, such as the interaction with circumstellar disks and the accretion of residual matter, or the presence of companions and so on. In the following, I will first overview the uncertainties *intrinsic* to the models, and then discuss the effects of the environment.

4.1. COMPARISON OF TRACKS

Several recent studies have reconsidered the PMS evolution of stars with population I compositions over a wide mass range (e.g. D'Antona & Mazzitelli 1994, 1997; Forestini 1994; Swenson et al. 1996; Baraffe et al. 1997; Palla & Stahler 1999). The main motivation for these studies is the progress in the fields of the equation of state, radiative opacities and the treatment of convection, each of which greatly influences the surface properties, i.e. the observables, of PMS stars. Before summarizing the main properties of the new models, let first stress the following point: the average error in the determination of the observable quantities, $L_{\rm bol}$ and $T_{\rm eff}$, is of the same order of magnitude than the theoretical ones. Typically, $\Delta T_{\rm eff}=\pm 300$ K and $\Delta \log\ (L_*/L_\odot)=\pm 0.25$ dex, for stars observed in the nearby star forming regions (e.g. Strom & Strom 1994). On the other hand, the mean spacing between Hayashi tracks is of the order of $\sim$130 K for $M_*=0.5\ M_\odot$, and of only $\sim$60 K for a 1 $M_\odot$ star (Forestini 1994). Thus, for very young stars, still on the vertical portion of the tracks, the mass assignement based on their position can lead to errors of a factor of 2.

The largest sources of uncertainty in the position of the tracks in the H-R diagram are due to the poor description of turbulent convection and the limited knowledge of low-temperature opacities. In addition, to construct an H-R diagram, one should derive $T_{\rm eff}$ and $L_{\rm bol}$ from observable quantities. The derivation of $T_{\rm eff}$ relies on temperatures scales which are fairly well known for dwarfs between A and K types. For M dwarfs ($T_{\rm eff}\lesssim 4000$ K), differences between temperature scales are much larger (Allard et al. 1997). The problem is that there are only two eclipsing binary systems, YY Gem (M0.5, 3770K) and CM Dra (M4.5, 3150 K), with accurately measured temperatures. Thus, it is difficult to plot a reliable H-R diagram for the low- and very low-mass stars and obtain good mass and age estimates. This warning is particularly important when attempting to derive the initial mass function in nearby star forming regions. An example is provided by the recent study of Luhman & Rieke (1998) of the the low-mass end of the IMF in L1495E in Taurus. They find *very* different results depending on the choice of the set of tracks: an object with a mass of 0.25 $M_\odot$ using D'Antona & Mazzitelli (1994) tracks corresponds to a 0.5 M_* using Baraffe et al. (1997) tracks. Thus, the shape of the IMF, as well as the star formation history, cannot be univoquely determined. The lesson is clear: it is still premature to draw firm conclusions from observations of the low mass end of the stellar distribution with the current uncertainties in both evolutionary tracks and in the conversion from observational to theoretical quantities (see also the discussion in D'Antona & Mazzitelli 1998).

4.2. LITHIUM DEPLETION

The depletion of lithium in both young and evolved stars is considered one of the strongest constraints imposed on stellar evolution theory. The surface abundances in fact provide a critical test for the physical processes (convection, opacity, rotation, mass loss) which ought to be included in the theoretical models in order to reproduce the observed level of depletion. Due to its small binding energy, ^{7}Li (the most abundant of the two stable isotopes of lithium) is easily destroyed in stellar interiors via the reaction ^{7}Li(p,α)^{4}He at temperatures around 2.5×10^6 K. According to standard models, depletion occurs only when the outer convection extends down to that temperature. Thus, it appears quite unavoidable that some ^{7}Li depletion due to nuclear burning takes place already during PMS contraction. Other processes, associated with the mixing due to transport of angular momentum through the star, are effective on much longer time scales and dominate the depletion history during the main sequence phase (e.g. Forestini 1994; Martin & Claret 1996; Venturi et al. 1998).

The theoretical predictions are rather well established, independently of the adopted models. Stars more massive than 1.7 $M_\odot$ should *not* show any ^{7}Li depletion at all; solar-type stars are significantly depleted, while for sub-solar stars there should be no ^{7}Li left over (e.g. Forestini 1994). For stars with $M_*\gtrsim0.5$ $M_\odot$, most lithium burns after convection has halted in the stellar core. Predictions of lithium depletion then depend on the temperature at the bottom of the convection zone, whose exact location is sensitive to opacity, convection, and rotation. Stars with $M_*\lesssim0.5$ $M_\odot$ are fully convective during lithium burning. Since the rate of contraction of such stars is controlled by the effective temperature, the amount of lithium depletion is also sensitive to $T_{\rm eff}$ and hence to the surface opacities. Several groups have followed numerically the phase of lithium burning, and the models make specific predictions about the time evolution of the lithium depletion boundary. At ages 30, 70 and 140 Myr, the lithium depletion edge should occur at 0.17 $M_\odot$, 0.09 $M_\odot$ and 0.07 $M_\odot$ (Baraffe et al. 1997; Burrows et al. 1997; D'Antona & Mazzitelli 1997). To bypass the uncertainties of numerical models, Bildsten et al. (1997) have developed a clever analytic approach based on the fact that $T_{\rm eff}$ remains approximately constant during the fully convective phase (see the low-mass tracks of Fig. 5). Rather than calculating $T_{\rm eff}$, Bildsten et al. calculate the dependence of lithium depletion on $T_{\rm eff}$, obtaining the radius, age and luminosity of a PMS star as a function of lithium depletion. This method can be used to derive the age of open clusters with higher accuracy than any other method.

One of the most successful applications of the theory of Li-burning has been in the field of brown dwrafs. The limiting mass for ^{7}Li-burning is $M_* \geq 0.06$ $M_\odot$, since degeneracy effects in lower mass stars prevent the onset of nuclear reactions (D'Antona & Mazzitelli 1994). This value is below the substellar mass limit, usually taken between 0.08 and 0.07 $M_\odot$. Thus, it has been suggested that the presence of lithium lines in the observed stellar spectra can be used as a powerful probe to search for brown dwarf candidates (Rebolo, Martin & Magazzù 1992). The Li-depletion history for different masses is shown in Figure 7. Using this diagnostic, the first brown dwarfs have been discovered in the Pleiades (Rebolo et al. 1996; Basri, Marcy & Graham 1996) and about a dozen candidates have been identified to date (Martin et al. 1998; Stauffer et al. 1998).

4.3. EFFECTS OF MASS ACCRETION

The evolution described so far, although improved by the account of more realistic initial conditions and input physics, is still rather conventional. It assumes that each star evolves in isolation at constant mass from the birthline to the arrival on the main sequence. But we know that in reality the situation is more complex, owing to the interaction of the star with the environment. An important effect to consider is the occurrence of residual mass accretion from a circumstellar disk during the PMS phase. Accretion alters the total (star+disk) luminosity, the evolutionary path, and hence the age estimate of a star. Hartmann, Cassen & Kenyon (1997) have presented a detailed analysis of the effects of disk accretion on the initial evolution of fully convective low-mass PMS stars.

Current estimates of mass accretion rates derive from the analysis of the excess optical continuum radiation in T Tauri and Herbig stars that also show an infrared excess. The latter is interpreted as being due to the presence of an active circumstellar disk. In this case, the disk luminosity is the sum of two contributions,

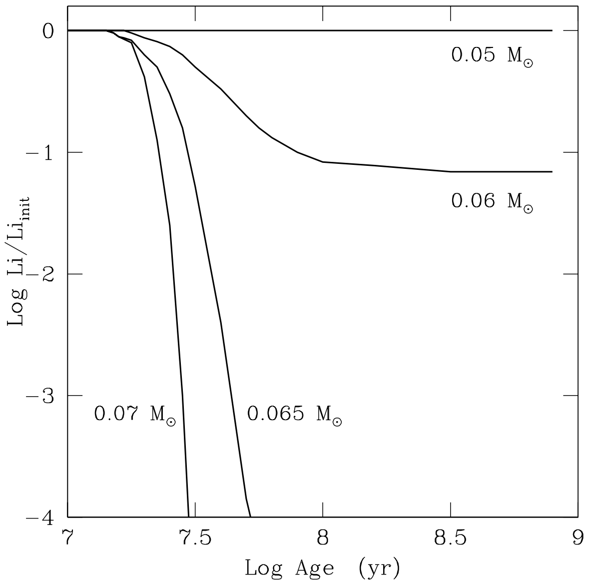

Figure 7. ^{7}Li-depletion as function of time for stars in the mass range 0.07 to 0.05 M$_\odot$. (From Rebolo et al. 1995)

$$L_{\rm disk} = \frac{GM_*\dot{M}_{\rm acc}}{2R_*} + L_{\rm rep}, \tag{25}$$

where the first term represents the accretion luminosity, while the second term is due to the absorption and reradiation of light from the central star. Typically, $L_{\rm rep}$ ~0.25-0.5 L$_*$. Thus, unless $L_{\rm disk} \geq L_*$, the identification of the excess luminosity as *accretion* is not secure. On the other hand, observations indicate that at most $L_{\rm disk}$ ~0.5 L$_*$.

If the optical excess is assumed to arise in a boundary layer (BL) between the star and a disk, then the standard theory of viscous accretion disks predicts that up to half of the accretion luminosity is emitted as radiation,

$$L_{\rm BL} \leq \frac{GM_*\dot{M}_{\rm acc}}{2R_*}. \tag{26}$$

Thus, measurements of $L_{\rm BL}$ can provide a direct estimate of the amount of mass actually falling onto a star. Measurements of the veiling in a large sample of T Tauri stars yield values in the range $\dot{M}_{\rm acc}$=10^{-8}–10^{-7} M$_\odot$ yr^{-1} (Hartmann & Kenyon 1990; Bertout & Regev 1992). Higher values of $\dot{M}_{\rm acc}$, up to 100 times, have been derived for the more massive Herbig

Ae/Be stars (e.g. Hillenbrand et al. 1992). Note, however, that in the absence of angular momentum loss, accretion at these rates would spin up the central star to half the break-up velocity in a few million years. Since young stars are known to rotate at typically 1/10–1/5 of the break-up speed (e.g. Bouvier, Forestini & Allain 1998), it is likely that strong winds carry away the angular momentum excess. Therefore, it is still not clear what fraction of the accreted mass is actually incorporated into the star.

The question, then, is whether the inferred rates are high enough to modify the evolutionary tracks. Hartmann & Kenyon (1990) argue that indeed the path is greatly affected, and estimate from qualititative arguments that about 10% of the final mass of a T Tauri is accreted during the PMS phase. Simple energy considerations allow to derive an estimate of the effect of mass accretion on fully convective stars (e.g. Palla 1994; Hartmann, Cassen & Kenyon 1997). The evolution of the stellar luminosity is described by the equation

$$\frac{d}{dt}\left(-\frac{3GM_*^2}{7R_*}\right) = -L_* - \frac{GM_*\dot{M}_{\rm acc}}{R_*} + \dot{M}_{\rm acc}\delta \ , \tag{27}$$

where the term on the lhs represents the temporal change of the gravitational potential energy; the second and third terms on the rhs express the gain of (negative) energy by mass accretion and the released luminosity of freshly accreted deuterium. This equation can be recast in the form of a nondimensional differential equation, whose solution is straightforward. To test the effect of mass accretion, the evolution of stars with initial mass of 0.6 and 1.0 $M_\odot$ has been followed allowing for steady mass accretion at different rates for the first 3 million years (Parigi 1992). The result is that, as long as the value of $\dot{M}_{\rm acc}$ remains below $\sim 10^{-7}$ $M_\odot$ yr^{-1}, the new tracks do not differ substantially from those computed at constant mass. Moreover, if the *global* effect of mass accretion is limited to about 10% of the final mass, it would take only 1 million years to a 1 $M_\odot$ star to accrete such an amount of mass at $\dot{M}_{\rm acc}=10^{-7}$ $M_\odot$ yr^{-1}. Small departures can be appreciated only after at least 2 million years for $\dot{M}_{\rm acc}=10^{-7}$ $M_\odot$ yr^{-1}, implying that, unless accretion continues for a substantial part of the PMS evolution at high rates, the uncertainty in the location of a star in the H-R diagram due to this effect is small. Following a different approach, Siess & Forestini (1996) and Siess, Forestini & Bertout (1997) have computed the evolution of stars that accrete a substantial part of their final mass during the PMS phase. Clearly, in such a case the evolutionary tracks are greatly affected: compared to a non-accreting star, the evolution is accelerated, the central temperature remains larger, and the star appears systematically younger (with age estimates affected by up to factors 2 to 3). Although the physical effects are well understood, it remains to be seen if the assumption that most of the mass is accreted during PMS evolution is confirmed by observations.

4.4. EFFECTS OF BINARIES

The study of PMS binaries offers the best way to test the theoretical evolutionary tracks. The measurement of the dynamical mass of the components of any binary system would yield in fact an absolute mass calibration of the tracks, and thus provide a direct answer for the exact location of the tracks in the H-R diagram. The progress in the field of PMS binaries has been tremendous (e.g. Mathieu 1994). The population of binary systems in the nearest star forming regions has now been studied and a binary frequency of at least 50% has been derived for systems with angular separations in the range 3 to 1400 AU. It appears that there is even an excess of such systems in comparison to what found among nearby solar-type stars, possibly implying that binary formation is the main mode of star formation (Simon et al. 1995).

Unfortunately, there are very few cases where it has been possible to derive the dynamical mass of the components of an eclipsing binary system. One such case is TY CrA, a binary with a period of 2.89 days in the Corona Australis complex (Beust et al. 1997; Casey et al. 1998). Accurate spectroscopic measurements allow to derive the masses of the individual components, M_1=3.16 $M_\odot$ and M_2=1.64 $M_\odot$. The position of TY CrA in the H-R diagram is shown in Figure 8. The primary appears slightly below the ZAMS, near a mass of 3.0 $M_\odot$. This value compares well with the more precise spectroscopic determination of 3.16 $M_\odot$. The secondary indeed falls just above the 1.5 $M_\odot$ evolutionary track. Thus, the two methods (spectroscopic and photometric) for obtaining the component masses are in essential agreement. What about the stellar ages? Unfortunately, the location of the primary so close to the ZAMS makes it impossible to assign a reliable contraction age. However, the star illuminates a bright reflection nebula in the Corona Australis cloud, and the system's spectral energy distribution rises in the mid-infrared regime toward longer wavelengths. Thus, the primary is undeniably young, a typical Herbig Be star situated within both interstellar and circumstellar gas and dust. Suppose we tentatively assign it the pre-main-sequence age for a 3 $M_\odot$ star just arriving on the ZAMS, or 2×10^6 yr. Then, the corresponding isochrone (dashed curve in Fig. 8) passes close to the secondary's position. The components of TY CrA are therefore plausibly coeval, although the data do not permit a more quantitative assessment. Age assignments are more trustworthy when both stars lie well above the ZAMS. No eclipsing binaries of this kind are known, but there are a number of non-eclipsing, double-lined systems. In the absence

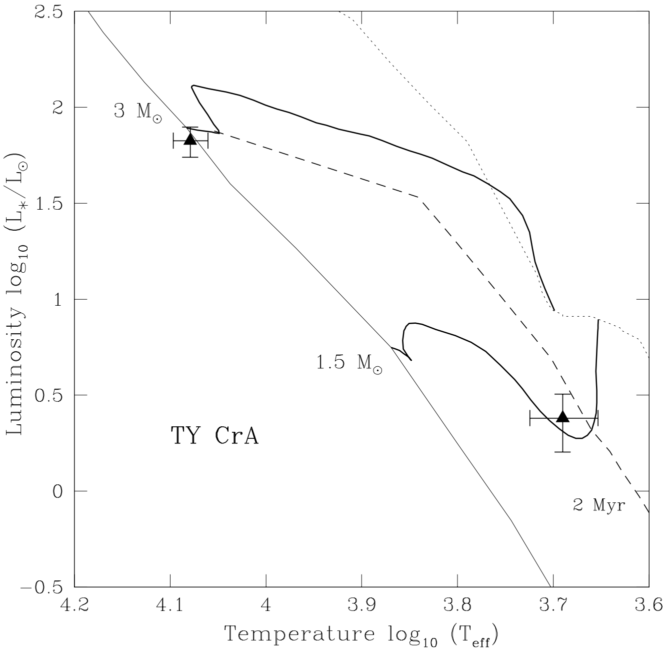

Figure 8. Location of TY CrA in the H-R diagram. Stellar parameters are from Casey et al. (1998). Evolutionary tracks, isochrone and birthline are from Palla & Stahler (1999).

of eclipses, one must obtain T_{eff} and L_{bol} for each star by careful analysis of both the composite SED and the shifting, narrow-band spectrum.

Discerning the relative luminosities from an unresolved pair of stars is no simple matter, and the foregoing results are subject to some uncertainty. The situation further improves when we consider wider, spatially resolved binaries. In this case, however, we have no spectroscopic mass ratios for comparison. Studies conducted in several nearby star forming regions have shown that most of the pairs when placed on the H-R diagram apper to be coeval, within the observational errors, (Hartigan, Strom & Strom 1994; Brandner & Zinnecker 1997). This implies that binary systems consist of stars that were born nearly simultaneously. Thus, the typical binary must arise *in situ*, rather than through capture.

4.5. THE INSTABILITY STRIP FOR PMS STARS

I will conclude this chapter with a discussion of a potentially important, but not yet fully explored aspect of PMS evolution: the pulsational properties of PMS stars. The fact that young stars during their evolution to the MS move across the instability region of post–MS stars raises the possibility that even a PMS could indeed pulsate (e.g. Baade & Stahl 1989). It is known that stars over essentially the whole mass spectrum can become pulsationally unstable during various stages of their evolution (Gautschy & Saio 1996). In particular, δ Scuti stars are intermediate-mass variables of spectral type A to F with pulsation periods less than $0\overset{d}{.}3$ and light amplitudes ranging from thousandths of magnitude to some tenths (Breger 1979). In spite of the traditional association of δ Scuti pulsation with stars in their core hydrogen-burning phase or evolving towards the base of the giant branch and burning hydrogen in a shell, some δ Scuti have been identified to be PMS objects. The best examples are two Herbig Ae stars, HR 5999 (Kurtz & Marang 1995) and HD 104237 (Donati et al. 1997). For HR 5999, the peak-to-peak pulsation amplitude is of about $0\overset{m}{.}013$ in Johnson V-band with a period of 4.99 hr, superimposed on a nonperiodic photometric variation of $0\overset{m}{.}35$. In HD 104237, the period of pulsation is approximately 40 minutes and the velocity amplitude about 1 km sec^{-1}.

Figure 9 shows the location of the boundaries of the instability strip for PMS computed by Marconi & Palla (1998). The red edge varies between ∼6500 K and ∼7100 K, whereas the blue edge between ∼7100 K and ∼7500 K. The width of the strip is nearly constant and equal to about 650 K. All the models on the red edge are pulsating in the fundamental mode, while those on the blued edge in either of the overtone modes. The time spent by each star within the strip is also a constant fraction of the total PMS contraction time, typically between 5 and 10%, although in absolute terms it decreases from $\sim 10^6$ yr for $M_*=1.5\ M_\odot$ to 8×10^4 yr for $M_*=4\ M_\odot$. Despite the relatively short times, Fig. 9 shows that about a dozen known Herbig Ae/Be stars have the right combination of luminosity and temperature to qualify as candidate pulsators. Searches for δ Scuti type variability in these stars are already under way. It is expected that the additional information provided by the detection of a larger number of pulsating stars will help constraining the internal structure of young stars and testing evolutionary models.

Acknowledgements

I am grateful to Steve Stahler who has worked with me on many aspects of the work presented in this review. I wish to acknowledge the frutiful collaboration with Marcella Marconi on the pulsational instability of PMS stars. It is a pleasure to thank Nick Kylafis and Charlie Lada for their kind invitation to attend Crete II. Partial support was provided by CNR grant 97.00018.CT02 to the Osservatorio di Arcetri.

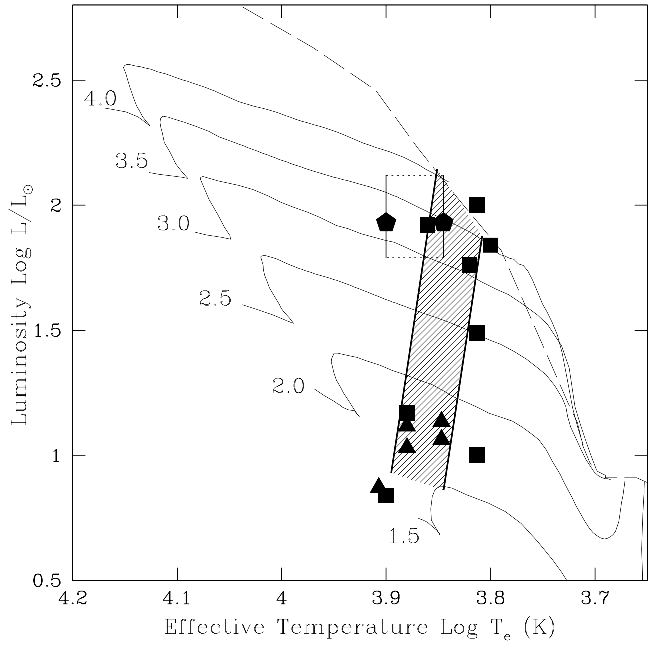

Figure 9. The shaded shows the location of the instability strip of PMS stars in the HR diagram. The various symbols indicate the distribution within or near the boundaries of the instability strip of known PMS stars that can be considered candidates for pulsational instability.

References

Alexander, D.R., Ferguson, J.W. 1994, *ApJ*, **437**, 879
Alexander, D.R., Augason, G.C., Johnson, H.R. 1989, *ApJ*, **345**, 1014
Alexander, D.R., Tamanai, A.I., Allard, F., Ferguson, J.W. 1998 *BAAS*, **67**, 16
Allard, F., Hauschildt, P.H., Alexander, D.R., Starrfield, S. 1997, *ARAA*, **35**, 137
Anders, E., Grevesse, N. 1989, *Geochim. Cosmochim. Acta*, **53**, 197
Baade, D., Stahl, O. 1989, *A&A*, **209**, 268
Baraffe, I., Babrier, G., Alla, F., Hauschildt, P.H. 1997, *A&A*, **327**, 1054
Basri, G., Marcy, G.W., Graham, J.R. 1996, *ApJ*, **458**, 600
Beech, M., Mitalas, R. 1995, *ApJS*, **95**, 517
Bernasconi, P., Maeder, A. 1996, *AA*, **307**, 829
Bertout, C., Regev, O. 1992, *ApJ*, **399**, L163
Beust, H., Corporon, P., Siess, L., Forestini, M., Lagrange, A-M. 1997, *A&A*, **320**, 478
Bildsten, L. Brown, E.F., Matzner, C.D., Ushomirsky, G. 1997, *ApJ*, **482**, 442
Böhm-Vitense, E. 1958, *Z. f. Ap.*, **46**, 108
Bonnell, I., Bate, M.R., Zinnecker, H. 1998, *MNRAS*, **298**, 93
Bouvier, J., Forestini, M., Allain, S. 1997, *A&A*, **326**, 1023
Brandner, W., Zinnecker, H. 1997, *A&A*, **321**, 220
Burrows, A., Marley, M., Hubbard, W., Lunine, J., Guillot, T., Saumon, D., Freedman, R., Sudarsky, D., Sharp, C. 1997, *ApJ*, **491**, 856
Canuto, V.M., Mazzitelli, I. 1991, *ApJ*, **370**, 295

Canuto, V.M., Goldman, I., Mazzitelli, I. 1996, *ApJ*, **473**, 550
Casey, B.W., Mathieu, R.D., Vaz, L.P.R., Andersen, J., Suntzeff, N.B. 1998, *AJ*, **115**, 1617
Caughlan, G., Fowler, W. 1988, *Atomic Data Nucl. Data Tables*, **40**, 283
Cox, J.P., Giuli, R.T. 1968, *Principles of Stellar Structure*, **II**, (New York: Gordon and Breach)
Cox, A.N., Tabor J.E. 1976, *ApJS*, **31**, 271
D'Antona, F. 1993, *Inside the Stars*, eds. W.W. Weiss & A. Baglin, A.S.P. Conf. Ser. 40 (San Francisco: Astr. Soc. Pac.), p.395
D'Antona, F., Mazzitelli, I. 1984, *A&A*, **138**, 431
D'Antona, F., Mazzitelli, I. 1997, priv. comm.
D'Antona, F., Mazzitelli, I. 1998 *Cool Stars in Clusters and Associations*, eds. G. Micela, R. Pallavicini and S. Sciortino , *Mem.S.A.It.*, **68**, 807
Däppen, W. 1993, *Inside the Stars*, eds. W.W. Weiss & A. Baglin, A.S.P. Conf. Ser. 40 (San Francisco: Astr. Soc. Pac.), p.208
Donati, J.-F., Semel, M., Carter, B.D., Rees, D.E., Collier Cameron, A. 1997, *MNRAS*, **291**, 658
Draine, B.T., Lee, H.M. 1984, *ApJ*, **285**, 89
Ezer, D., Cameron, A.G.W. 1965, *Canadian J. Phys.*, **43**, 1497
Forestini, M. 1994, *A&A*, **285**, 473
Gaustad, J.E. 1963, *ApJ*, **138**, 1050
Gautschy, A., Saio, H. 1996, *ARAA*, **34**, 551
Graboske, H., DeWitt, H.E., Grossman, H.S., Cooper, M.S. 1973, *ApJ*, **181**, 457
Grossman, A.N., Graboske, H.C. 1971, *ApJ*, **164**, 475
Hartigan, P., Strom, K.M., Strom, S.E. 1994, *ApJ*, **427**, 961
Hartmann, L., Kenyon, S.J. 1990, *ApJ*, **349**, 190
Hartmann, L., Cassen, P., Kenyon, S.J. 1997, *ApJ*, **475**, 770
Hayashi, C. 1966, *ARAA*, **4**, 171
Henyey, L.G., LeLevier, R., Levee, R.D. 1955, *Pub. A.S.P.*, **67**, 154
Hillenbrand, L.A., Strom, S.E., Vrba, F.J., Keene, J. 1992, *ApJ*, **397**, 613
Huebner, W.F., Merts, A., Magee, N.H., Argo, M.F. 1977, *Los Alamos Sci. Lab. Rep.*, LA-6760-M
Iben, I. 1965, *ApJ*, **141**, 993
Iglesias, C.A., Rogers, F.J. 1991, *ApJ*, **371**, L73
Iglesias, C.A., Rogers, F.J. 1996, *ApJ*, **464**, 943
Kahn, F.D. 1974, *A&A*, **37**, 149
Kurtz, D.W., Marang, F. 1995, *MNRAS*, **276**, 191
Larson, R.B. 1969, *MNRAS*, **145**, 121
Larson, R.B. 1972, *MNRAS*, **157**, 121
Larson, R.B., Starrfield, S. 1971, *A&A*, **13**, 190
Luhman, K.L., Rieke, G.H. 1998, *ApJ*, **497**, 354
Marconi, M., Palla, F. 1998, *ApJ*, **507**, L141
Martin, E.L., Claret, A. 1996, *A&A*, **306**, 408
Martin, E.L., Basri, G., Zapatero Osorio, M.R., Rebolo, R., López, R.J., Garcia, R.J. 1998, *ApJ*, **507**, L41
Mathieu, R.B. 1994, *ARAA*, **32**, 465
Mazzitelli, I. 1989, *Low-Mass Star Formation and Pre–Main-Sequence Objects*, ed. Bo Reipurth, ESO Proc. 33, p.407
Mazzitelli, I., Moretti, M. 1980, *ApJ*, **235**, 955
Mihalas, D., Däppen, W., Hummer, D.G. 1988, *ApJ*, **331**, 815
Nakano, T. 1989, *ApJ*, **345**, 464
Palla, F. 1994, *Infrared Astronomy*, eds. A. Mampaso & F. Sanchez (Cambridge: Cambridge Univ. Press), p.1
Palla, F., Stahler, S.W. 1990, *ApJ*, **360**, L47
Palla, F., Stahler, S.W. 1991, *ApJ*, **375**, 288

Palla, F., Stahler, S.W. 1993, *ApJ*, **418**, 414

Palla, F., Stahler, S.W. 1999, *ApJ*, in press

Parigi, G. 1992, Thesis, Univ. of Florence, unpublished

Pollack, J.B., Hollenbach, D., Beckwith, S., Simonelli, D.P., Roush, T., Fong, W. 1994, *ApJ*, **421**, 615

Rebolo, R., Magazzù, A., Martin, E.L. 1995, *Stellar and interstellar lithium*, eds. F. Spite and R. Pallavicini, *Mem.S.A.It.*, **66**, 375

Rebolo, R., Martin, E.L., Magazzù, A. 1992, *ApJ*, **389**, L83

Rebolo, R., Martin, E.L., Basri, G., Marcy, G.W., Zapatero Osorio, M.R. 1996, *ApJ*, **469**, L53

Rogers, F.J., Iglesias, C.A. 1992, *ApJS*, **79**, 507

Salpeter, E.E. 1954, *Mem. Roy. Soc. Liège*, **14**, 116

Schaller, G., Schaerer, D., Meynet, G., Maeder, A. 1992, *A&AS*, **96**, 269

Seaton, M.J. 1993, *Inside the Stars*, eds. W.W. Weiss & A. Baglin, A.S.P. Conf. Ser. 40 (San Francisco: Astr. Soc. Pac.), p.222

Seaton, M.J., Yan, Y., Mihalas, D., Pradhan, A.K. 1994, *MNRAS*, **266**, 805

Siess, L., Forestini, M. 1996, *A&A*, **308**, 472

Siess, L., Forestini, M., Bertout, C. 1997, *A&A*, **308**, 472

Simon, M., Ghez, A.M., Leinert, Ch. et al. 1995, *ApJ*, **443**, 625

Simon, N. 1982, *ApJ*, **260**, L87

Stahler, S.W. 1983, *ApJ*, **274**, 822

Stahler, S.W. 1988a, *ApJ*, **332**, 804

Stahler, S.W. 1988b, *Pub. A.S.P.*, **100**, 1474

Stahler, S.W., Walter, F.M. 1993, *Protostars and Planets III*, eds. E.H. Levy & J.I. Lunine (Tucson: The Univ. of Arizona Press), p.405

Stahler, S.W., Shu, F.H., Taam, R.E. 1980, *ApJ*, **302**, 590

Stahler, S.W., Palla, F., Ho, P.T.P. 1999, *Protostars and Planets IV*, eds. V. Mannings, A.P. Boss, and S.S. Russell (Tucson: U. of Arizona Press), in press

Stauffer, J.J.R., Schultz, G., Kirkpatrick, J.D. 1998, *ApJ*, **499**, L199

Strom, K.M., Strom, S.E. 1994, *ApJ*, **424**, 237

Swenson, J.H., Faulkner, J., Rogers, F.J., Iglesias, C.A. 1996, priv. comm.

Venturi, P., Zeppieri, A., Mazzitelli, I., D'Antona, F. 1997, *A&A*, **331**, 1011

Von Sengbusch, K. 1968, *Zs. f. Ap.*, **69**, 79

Winkler, K.H., Newman, M.J. 1980, *ApJ*, **236**, 201